Structural properties and energetics of intrinsic and Si-doped GaAs nanowires: First-principles pseudopotential calculations

Nahid Ghaderi,[1,2] Maria Peressi,[1,3] Nadia Binggeli,[4,5] and Hadi Akbarzadeh[2]
[1]*Theory@Elettra Group, CNR-INFM DEMOCRITOS National Simulation Center, Trieste, Italy*
[2]*Department of Physics, Isfahan University of Technology, 84156 Isfahan, Iran*
[3]*Department of Physics, University of Trieste, Strada Costiera 11, I-34151 Trieste, Italy*
[4]*The Abdus Salam International Centre for Theoretical Physics, Strada Costiera 11, I-34151 Trieste, Italy*
[5]*CNR-INFM DEMOCRITOS National Simulation Center, Trieste, Italy*
(Received 21 July 2009; revised manuscript received 25 January 2010; published 15 April 2010)

We investigate by first-principles pseudopotential calculations the structural properties and the energetics of undoped and Si-doped unpassivated GaAs nanowires (NWs). On the basis of total energy calculations for the undoped NWs as a function of diameter we find that, in contrast to the bulk phase, wurtzite (WZ) NWs are more stable than zincblende (ZB) NWs for diameters up to about 50 Angstrom. We also investigate the preferential position of Si dopants in GaAs WZ NWs: we find that donors segregate to the surface, while acceptors prefer inner positions. On the basis of the formation energy study, the stability ranges for Si donor and acceptor sites are similar to the bulk ZB case, with a slight increase in the stability range for donor sites. However, in contrast to acceptors, donors preferentially segregate to surface dangling-bond sites at large NW diameters, and act as deep impurities, rather than shallow donors, thus hindering *n*-type conductivity. This could contribute to explain the preferential *p*-type behavior which was observed in recent experiments on Si-doped NWs grown by molecular-beam epitaxy, in addition to other possible effects, including, e.g., the kinetics of Si incorporation.

DOI: 10.1103/PhysRevB.81.155311 PACS number(s): 61.46.Km, 71.15.−m, 71.55.−i, 73.22.−f

I. INTRODUCTION

Semiconductor nanowires (NWs) offer nowadays new perspectives for nanoelectronic devices. Recently, high-quality GaAs NWs have been experimentally grown on different substrates: they are regularly shaped and nicely oriented, with wurzite (WZ) or zincblende (ZB) structure depending on the substrate and on the growth conditions.[1–4] For instance, self-assembled GaAs NWs grown on Si(111) substrate with or without Ga predeposition have predominantly WZ or ZB structure, respectively.[4] Such polytypism is a peculiar feature of III–V NWs at variance with the bulk phase. In the case of bulk GaAs, in particular, the energy difference between the metastable WZ and the stable ZB phase obtained in computational studies[5–7] is somewhat larger than in other III–V systems, and until very recently[8] only the ZB phase could be produced experimentally.

The polytypism in III–V NWs has been recently addressed by several theoretical models accounting for the growth thermodynamics.[9,10] A systematic investigation of the relative stability of clean ZB and WZ III–V NWs based on an empirical potential approach has also been presented,[11] predicting for GaAs a critical diameter of about 15 nm up to which WZ NWs are more stable. So far, however, to the best of our knowledge no *ab initio* calculation of the energetics and structural properties of clean WZ and ZB GaAs NWs has been reported. First-principles pseudopotential investigations have addressed the stability of clean InP ZB and WZ NWs,[12,13] and very recently the surface energies of both clean and passivated ZB and WZ InAs NWs have also been examined by *ab initio* computations, as well as the surface energies of several passivated GaAs and InP WZ and ZB NWs.[14] The results of these calculations indicate that while for clean NWs, WZ NWs are more stable than ZB NWs in the limit of small diameters, for passivated NWs the relative stability at small diameters depends on the chemical potential of the passivating molecules. It should be mentioned, in this connection, that in the case of metal organic chemical vapor deposition growth, the experimental NWs are likely to be passivated, whereas in the case of molecular-beam epitaxy (MBE) growth, the NWs are unlikely to be passivated.[1–4,15]

Potential applications of semiconductor NWs as novel electronic devices critically depend on their doping properties. Doped GaAs NWs have been grown in the presence of several catalysts and substrates. However, information on the dopants incorporation and properties is still rather scarce. Si is a rather common dopant for GaAs, with amphoteric behavior in bulk GaAs,[16] although in typical MBE growth conditions, Si acts as *n*-type dopant. In Si-doped GaAs WZ NW's grown by MBE, however, surprisingly *p*-type doping has been experimentally observed.[3] The reason for this behavior is not known.

In general, the incorporation of impurities is a difficult task in nanocrystals. For dopants in semiconductor quantum dots, for example, "self-purification" mechanisms due to quantum confinement have been proposed based on density-functional calculations.[17–22] First-principles calculations have been performed for different doped NWs,[23–29] predicting in some, but not all, cases that impurities prefer to migrate toward the surface. For Si in GaAs NWs, however, no information is available on the preferred location of the impurities within the NWs.

In this paper, we present a comprehensive *ab initio* study of the energetics and structural properties of unpassivated GaAs NW with and without Si dopants. We find that the WZ

NWs are energetically favored with respect to ZB NWs for diameters up to 5 nm, and discuss their structural properties. We address the relative stability of the different donors and acceptors configurations within the WZ NWs, and based on our total energy and electronic structure calculations we propose a possible explanation for the *p*-type rather than *n*-type doping observed in MBE grown GaAs NWs.

II. COMPUTATIONAL DETAILS

Calculations have been performed within the framework of density-functional theory (DFT) in the local density approximation (LDA) assuming Ga 3*d* electrons frozen in the core using first-principles pseudopotentials to describe the valence electrons and plane waves as a basis set to expand the electronic wave functions. In order to check the robustness of our results, we performed also many tests using the generalized gradient approximation (GGA) instead of LDA and also assuming Ga 3*d* electrons in valence. Unless otherwise specified, the results reported in the following are LDA results with Ga 3*d* electrons in the core. Periodically repeated supercells are used for a convenient reciprocal space formulation of the problem. The QUANTUM-ESPRESSO package[30] and pseudopotentials publicly available[31] have been used. A kinetic energy cutoff of 26 Ryd ensures a good convergence of the results.

The theoretical lattice parameter of ZB GaAs is $a_0^{ZB}=5.56$ Å and those of WZ GaAs are $a_0^{WZ}=3.93$ Å and $c_0=6.44$ Å. The relative stability of the two bulk phases is correctly described by our numerical simulations, which predict a difference between the cohesive energy of the ZB and WZ phase of 11 meV/atom (12 meV/atom in GGA), in good agreement with the literature.[5–7] The calculated phonon contribution at $T=0$ is negligible (0.06 meV/atom, in the direction of reducing the difference).

We focus on NWs with ZB [111] and WZ [0001] growth directions. Along these directions, ZB and WZ structures are similar, but with a different stacking of anion-cation double layers: the stacking sequence for ZB is *abcabc*… and for WZ *ababab*… (see Fig. 1).

NWs oriented along these directions can naturally satisfy the constraints of charge-neutrality and nonpolarity of the exposed facets; NWs of this kind are in fact commonly reported.[3,32] A NW is characterized by its structure (ZB or WZ), its symmetry and shape around the growth axis [Triangular (T) or Hexagonal (H)] and the number of atoms in each double layer [(*na*,*nb*,*nc*) for ZB and (*na*,*nb*) for WZ].

We studied NWs with different kinds of nonpolar stoichiometric facets, namely the natural cleavage planes $(10\bar{1}0)$ and $(11\bar{2}0)$ for WZ (see Fig. 2), having only threefold coordinated atoms (we refer to them as DB1 atoms, i.e., atoms with one dangling bond),[33] and (110) and (112) planes for ZB, the former with threefold coordinated atoms only and the latter with threefold and twofold coordinated atoms (we refer to the twofold coordination as DB2, i.e., atoms with two dangling bonds). Each NW studied here is characterized by one type of facet, with equivalent termination. Most of the NWs considered have facets with DB1's only, namely, $(10\bar{1}0)$ for WZ and (110) for ZB NWs.

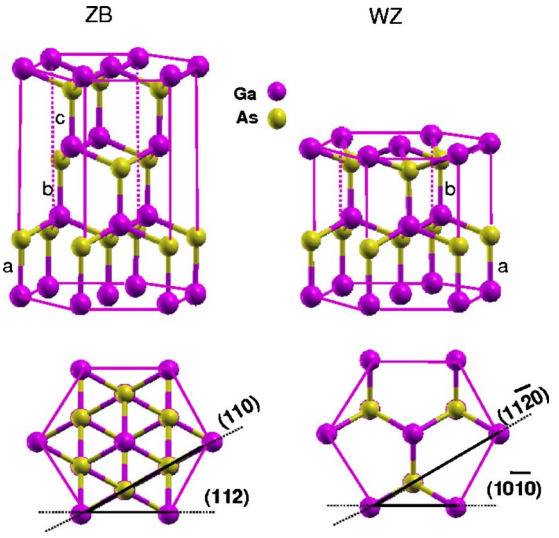

FIG. 1. (Color online) Ball and stick three-dimensional and top views of ZB and WZ structures along [0001] and [111] directions, respectively; *a*,*b*,*c* indicate the nonequivalent anion-cation double layers. In the top views, the natural cleavage (110) and (112) planes for ZB and $(10\bar{1}0)$ and $(11\bar{2}0)$ planes for WZ are indicated.

Periodically repeated hexagonal supercells with about 8–10 Å of vacuum space around the NW are used to minimize the interactions due to the artificial periodicity in the plane perpendicular to the growth axis. Supercells with unitary spacing $c=c_0$ ($c=\sqrt{3}a_0^{ZB}$) along the growth axis are used for undoped WZ (ZB) NWs, whereas for doped WZ NWs, calculations with longer ($c=2c_0$) cells are also performed to investigate the role of spacing between impurities. Brillouin zone integrations are carried out with smearing techniques using a $(1\times1\times4)$ *k*-point mesh for most of the NWs [a $(2\times2\times4)$ mesh for the smaller ones] and a Gaussian energy broadening of 0.01 Ry. Neutral impurity configurations are considered here.

We have studied the cohesive energy of WZ-H, WZ-T, and ZB-H GaAs NWs as well as, for comparison, that of their corresponding bulk phases, with respect to the separate bulk Ga and As phases. We have calculated the cohesive energy as

$$E_c=\left\{\sum_i n_i\mu_i-E_{tot}\right\}/\sum_i n_i, \tag{1}$$

where E_{tot} is the total energy of the simulation cell (the bulk one, or the one containing the GaAs NW), μ_i is the chemical

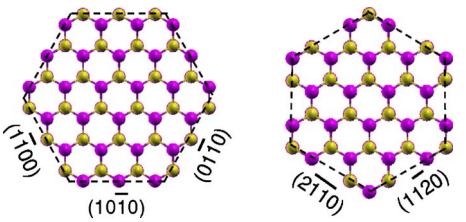

FIG. 2. (Color online) Ball and stick models of WZ-H(54,54) and WZ-H(42,42) NWs characterized by $(10\bar{1}0)$ and $(11\bar{2}0)$ facets, respectively. Top views are shown and for the sake of simplicity the atomic positions are unrelaxed.

TABLE I. Calculated energy gaps (in eV) for different WZ NWs and for bulks using different approximations (LDA/GGA, assuming Ga 3*d* electrons in core/valence). For each approximation, the gaps are calculated at the corresponding equilibrium theoretical lattice parameter (Ref. 42).

	LDA (Ga 3*d* core)		LDA (Ga 3*d* valence)		GGA (Ga 3*d* valence)	
NW	Indirect	Direct	Indirect	Direct	Indirect	Direct
WZ(6,6)	0.56	0.65	0.49	0.60	0.65	0.76
WZ(14,12)	1.29	1.49	1.15	1.39	1.26	1.35
WZ(24,24)	1.59	1.85	1.49	1.68		1.42
WZ(38,36)	1.43	1.72	1.29	1.50		1.20
WZ(54,54)	1.22	1.53	1.11	1.39		1.06
WZ(96,96)	0.99					
Bulk WZ		1.02		0.68		0.18
Bulk ZB	1.38	1.41		0.70		0.19

potential of atoms i (i=Ga or As), and n_i is the number of i atoms. The chemical potential of Ga and As is calculated using a eight-atom orthorhombic and a two-atom trigonal cell, respectively, representative of their bulk phase.

III. UNDOPED GAAS NANOWIRES

We have performed full supercell calculations for NWs with diameter up to about 27 Å, corresponding to the structure WZ-H(96,96). We point out that, in spite of the presence of DBs at surfaces, most of the GaAs NWs considered here are semiconducting. More precisely, all WZ NWs are semiconducting, whereas some ZB NWs with DB2 atoms at facet edges are found to be metallic or semimetallic. The energy gap depends on the type and diameter of NWs, but a general trend is clear: for WZ NWs, for instance, starting from the largest wire considered, WZ-H(96,96), the gap progressively increases with decreasing diameter, up to WZ-H(24,24), in agreement with quantum confinement. The gap then decreases, for smaller diameters, when the lateral size becomes comparable to the dimension of the GaAs surface unit cell (Table I).

Relaxations at facets are sizeable: As move outwards, Ga inwards, as shown in Fig. 3 for instance for the WZ-H(54,54) NW. This is similar to what we found in slabs calculations for the infinite $(10\bar{1}0)$ and $(11\bar{2}0)$ GaAs WZ surfaces and consistent with findings for other WZ NWs and nonpolar surfaces of binary semiconductor compounds.[13,34–37]

As an example, the structural parameters for the relaxed $(10\bar{1}0)$ infinite surface, with reference to Fig. 1 of Ref. 34 for their definition (see also Fig. 3), are: ω=17.2° (buckling angle), $d_{12,\perp}$=0.54 Å (minimum interlayer spacing between the first and second layer), d_0=1.28 Å (distance along the $[10\bar{1}0]$ direction between As and Ga atoms in the first and second layer, respectively), $d_{12,y}$=2.76 Å (distance between two closest Ga atoms in the first and second layer along the $[000\bar{1}]$ direction), $\Delta_{1,\perp}$=0.74 Å (distance along the $[10\bar{1}0]$ direction between As and Ga atoms in the first layer), $\Delta_{2,\perp}$=0.78 Å (distance along the $[10\bar{1}0]$ direction between As and Ga atoms in the second layer), and $\Delta_{1,y}$=2.18 Å (distance along the $[000\bar{1}]$ direction between As and Ga atoms in the first layer). These relaxations act in the direction of compensating DBs pushing surface states toward the band gap edges. Indications of surface states close to the band edges were already reported for instance for the $(10\bar{1}0)$ Cd-VI surfaces.[38]

Similar to findings reported in Ref. 13 for InP NWs, all GaAs NWs with diameter up to 27 Å that we have studied by full SCF calculations are more stable in WZ than in ZB structure (see Fig. 4). We note that the WZ-H(42,42) NW, which has $(11\bar{2}0)$ exposed facets, has a lower cohesive energy with respect to the WZ-T(38,36) and WZ-H(54,54) NWs of comparable size, which have instead $(10\bar{1}0)$ facets.[39] As we will show later, this is consistent with the higher formation energy of the $(11\bar{2}0)$ surface with respect to the $(10\bar{1}0)$ surface. Similarly, the ZB-H(38,24,24) NW with exposed (112) facets is less stable than the ZB-H(26,24,24) NW of comparable size with (110) facets, as one might expect from the presence of DB2 atoms at the (112) surface. It

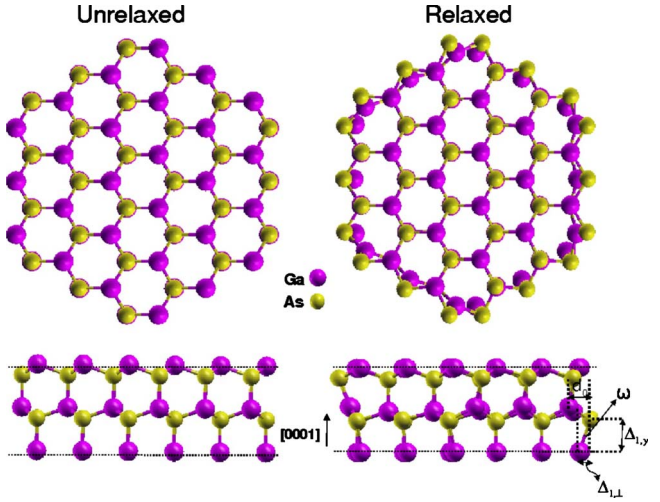

FIG. 3. (Color online) Ball and stick models of the WZ-H(54,54) NW characterized by $(10\bar{1}0)$ facets: unrelaxed (left) and relaxed (right) top and side views.

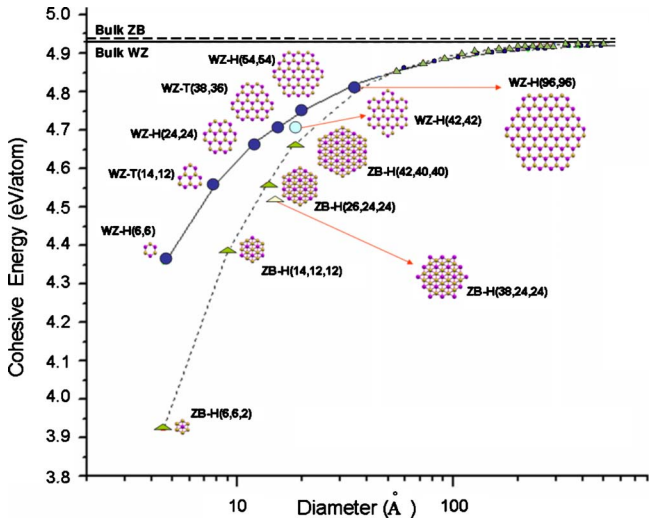

FIG. 4. (Color online) Cohesive energy [Eq. (1)] as a function of diameter for undoped GaAs nanowires with ZB and WZ structures. Large circles and triangles are from full SCF calculations; small symbols and interpolating lines are drawn according to Eq. (2). The bulk limits are also indicated. For the sake of simplicity, in these ball and stick models the atomic positions are unrelaxed.

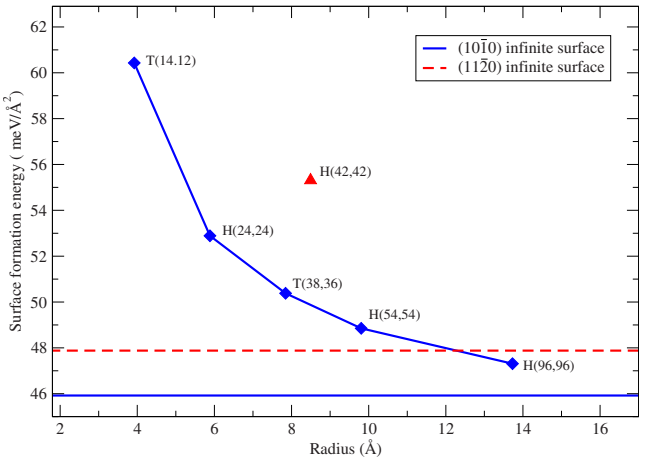

FIG. 5. (Color online) Surface formation energy as a function of the diameter of undoped GaAs WZ NWs characterized by (10$\bar{1}$0) and (11$\bar{2}$0) facets, compared with the corresponding infinite surfaces. Among the NWs with (11$\bar{2}$0) facets, only WZ-H(42,42) is reported here.

should be noted that ZB NWs with (110) facets also exhibit DB2 atoms, but only at facet edges.

The relative stability of the WZ and ZB NWs is mainly determined by the contribution of the different kinds of DBs at the NWs surface, which we can estimate from the SCF results. Following Ref. 13, we can express the NWs cohesive energy in terms of the DBs contributions,

$$E_c^{\mathrm{NW}}(\mathrm{WZ}) = E_c^{bulk}(\mathrm{WZ}) - \frac{N_{DB1}}{N_{tot}} E_{DB1}(\mathrm{WZ}),$$

$$E_c^{\mathrm{NW}}(\mathrm{ZB}) = E_c^{bulk}(\mathrm{ZB}) - \frac{N_{DB1}}{N_{tot}} E_{DB1}(\mathrm{ZB}) - \frac{N_{DB2}}{N_{tot}} E_{DB2}(\mathrm{ZB}) \tag{2}$$

where $E_c^{bulk}(\mathrm{ZB})$ is the cohesive energy of the bulk ZB (similarly for WZ), E_{DB1} and E_{DB2} are the energy contributions of threefold and twofold coordinated atoms, respectively, and N_{DB1} and N_{DB2} are their number in the NW. Fitting data obtained from full supercell NWs calculations it is possible to estimate E_{DB1} and E_{DB2}, which in turn can be used in Eq. (2) to extrapolate the cohesive energy for ZB and WZ NWs with larger diameters.

From the fit to the calculated cohesive energies of the WZ and ZB NWs with (10$\bar{1}$0) and (110) facets, respectively, we obtain: $E_{DB1}(\mathrm{WZ})=0.54$ eV, $E_{DB1}(\mathrm{ZB})=0.48$ eV, $E_{DB2}(\mathrm{ZB})=1.17$ eV. As expected, twofold coordinated atoms give a negative contribution to the cohesive energy which is about twice that of the threefold ones. On the basis of these values, we extrapolate that undoped WZ NWs are more stable than ZB NWs up to a diameter of at least 50 Å; for larger diameters (between 50 and 100 Å) the two types of NW structures become essentially degenerate within the numerical accuracy of the cohesive energy; for even larger diameters the DB contribution reduces with respect to the volume contribution, going toward the limit of the two corresponding bulk structures, with ZB slightly favored with respect to WZ. Similar results are obtained within the GGA: the WZ NWs are found to be more stable than the ZB NWs up to diameters of ~60 Å and the corresponding values of the fit are: $E_{DB1}(\mathrm{WZ})=0.37$ eV, $E_{DB1}(\mathrm{ZB})=0.37$ eV, and $E_{DB2}(\mathrm{ZB})=0.83$ eV.

The decreased stability of the WZ NW with (11$\bar{2}$0) facets, compared to WZ NWs with (10$\bar{1}$0) facets, can be understood based on the fact that the WZ (11$\bar{2}$0) surface has a somewhat larger formation energy, by 0.5 meV/a.u.^{2}, than the WZ (10$\bar{1}$0) surface. In Fig. 5, we show the corresponding surface formation energy E_s obtained as the difference between the total energy of the system (NW or slab) and the total energy of bulk GaAs with the same number of atoms, divided by the exposed area. The results for the sequence of NWs of increasing diameter, with (10$\bar{1}$0) facets, show a monotonous decrease of the surface formation energy toward the value of the corresponding infinite surface. A similar trend, with values systematically shifted toward higher energy is expected for NWs with (11$\bar{2}$0) facets, given the higher formation energy of the (11$\bar{2}$0) surface and the data for the WZ-H(42,42) NW.

IV. SI-DOPED GAAS WZ NWS

A. Impurity sites in the NWs

Given the peculiar amphoteric behavior of Si atoms in bulk GaAs, we consider also for NWs the possibility for Si to substitute either Ga or As atoms. We first focus in this subsection on the preferential position for each kind of dopant in a specific NW and then we discuss the role of the NW size. We devote the next subsection to the relative stability of donors with respect to acceptors as a function of the chemi-

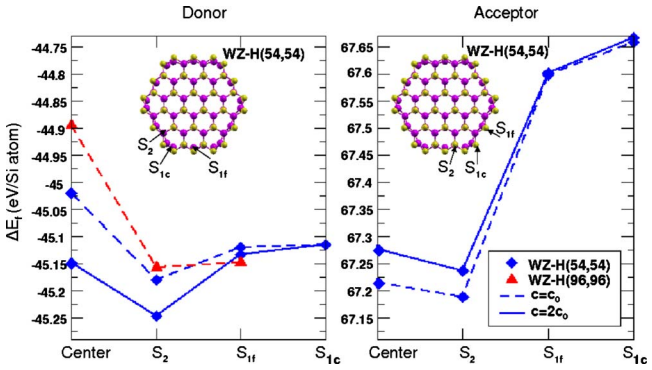

FIG. 6. (Color online) Si donor (left panel) and acceptor (right panel) relative formation energy in some NWs characterized by $(10\bar{1}0)$ facets. Results for centerlike, surface threefold, and subsurface fourfold coordinated positions (S_1 and S_2, respectively) are shown. A distinction is made for S_1: corner (S_{1c}) or middle of facets (S_{1f}) positions. Single ($c=c_0$) and double size ($c=2c_0$) structures along the NWs growth direction are compared.

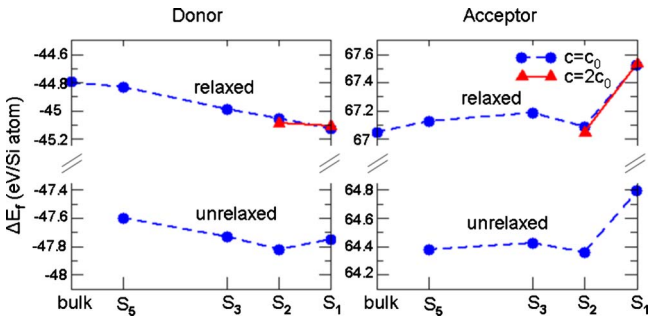

FIG. 7. (Color online) Si donor (left panel) and acceptor (right panel) relative formation energy in a slab with the $(10\bar{1}0)$ exposed surface in different positions with respect to the surface: first, second, third, and fifth layer. The value for the substitution in bulk is also reported for comparison. Comparison with the unrelaxed case (lower part) is also shown.

cal potentials involved. In view of the higher stability of the WZ NWs, with $(10\bar{1}0)$ facets, that we found for diameters up to 5 nm, with respect to ZB NWs, we focus here on the former type of NWs.

In Fig. 6, we examine the energetics of a Si substitutional impurity at different sites within a WZ-H(54,54) NW, in the case of Ga/donor sites (left-hand-side panel) and As/acceptor sites (right-hand-side panel). We reported, in these figures, the relative formation energy defined as the energy difference between the doped and the undoped system,[19]

$$\Delta E_f = E_{tot}^{doped} - E_{tot}^{undoped}. \quad (3)$$

The type of sites considered within the wire include bulklike or central positions, threefold coordinated sites within the surface layer (S_1), and fourfold coordinated sites within the subsurface layer (S_2). We examined wires with simple ($c=c_0$) and double impurity spacing ($c=2c_0$) along the growth direction. In the donor case, we also considered a larger WZ-H(96,96) NW. Lines are a guide to the eye collecting results for a specific NW. Focusing on the NW with the lowest doping (double spacing), we found that the most stable substitutional site for donors is the fourfold coordinated subsurface site S_2.

In NWs, the presence of corners can play a role not only in the energetics of intrinsic NWs (as clearly seen in Fig. 5), but also possibly in the energetics of defects. In the WZ-H(54,54) NW, we can distinguish between a threefold surface site close to the corner (S_{1c}) or in the middle of the facet (S_{1f}). In the donor case, the energy difference between S_{1c} and S_{1f} is however rather small. We further notice that the defect energy for the donor surface threefold site is only slightly sensitive to the separation between the impurities, consistent with the fact that the impurity electronic state is very localized, as we found from the electronic structure analysis. Donors in the fourfold site instead are found resonant with the bottom of the conduction band in our DFT calculations. We also observe that the energy difference between the S_1 surface sites and the S_2 subsurface site is small and decreases with increasing diameter of the wire, from the WZ-H(54,54) to the WZ-H(96,96) NW; the energy difference between the bulklike site and the S_2 site, instead, increases with increasing diameter, and is significant in the case of the WZ-H(96,96) NW.

Concerning acceptors, calculations performed for the WZ-H(54,54) NW indicate that their preferred position is the subsurface S_2 site, whereas, at variance with the donor case, the S_1 position is significantly higher in energy and the bulklike position is almost degenerate in energy with the S_2 site. Also for acceptors, the threefold S_1 site corresponds to a rather localized state, whereas the fourfold sites are related to states delocalized and resonant with the valence band.

The results for the energetics of donor (acceptor) impurities as a function of the site positions and wire size can be complemented by results for the impurity at or near the $(10\bar{1}0)$ infinite surface and within the bulk material. For the surface, we used a slab with 10 layers,[40] keeping the two central layers fixed, with 12.3 Å of vacuum space between consecutive slabs; we consider both (2×1) and (2×2) surface unit cells, corresponding to a separation of c_0 and $2c_0$ between the impurities along the c axis. To model the Si impurity in the bulk, we used an hexagonal supercell corresponding to a $(3\times3\times3)$ WZ unit cell ($a=3a_0$, $c=3c_0$) containing a single impurity. The corresponding relative formation energies, from the bulk to the surface, are shown in Fig. 7 for Si at donor (left-hand side panel) and acceptor (right-hand side panel) sites.

We find that the relative formation energy of Si donors progressively increases from the surface layer to the bulk, thus favoring surface segregation of donors. This trend is consistent with the higher formation energy found for the donor at the bulklike position in the wire with respect to the S_2 position. Moreover, the results in Fig. 7, which reflect a surface effect, can also explain the observed increase in the relative formation energy of the bulklike impurity in the wire when the diameter increases. Indeed, with increasing diameter, the distance of the bulklike impurity to the wire surface also increases, and based on the results in Fig. 7 this should lead to an increase in its formation energy. We note that in the WZ-H(54,54) NW, the S_2 donor site was somewhat fa-

vored with respect to the S_1 sites, both for $c=c_0$ and $c=2c_0$. However, comparison with the results for the NW with increased diameter and for the infinite surface indicates the S_1 sites become competitive (degenerate) in energy or even slightly favored in energy compared to the S_2 site at larger diameters. This is an important feature, as the S_1 site corresponds to a deep impurity, rather than a shallow donor that contributes to the *n*-type conductivity.

The results for the acceptors in the NW, and in particular the near degeneracy of bulklike and S_2 site and the substantially higher energy of the S_1 sites can similarly be explained based on the behavior we find for the impurity as a function of the position from the infinite surface. A small variation in energy is found going from the bulk to the S_2 surface sublayer site, whereas a large increase in energy is found for the S_2 sublayer surface site to the S_1 surface site. The results in Fig. 7 indicate that acceptors prefer fourfold positions, near the surface or within the bulk, whereas the S_1 sites are highly unfavored.

The results reported in Fig. 7 for the slabs with relaxed (upper panels) and unrelaxed (lower panels) positions also show the importance of relaxations, which change the relative stability of S_1 and S_2 sites for donors.

Notwithstanding all the details depending on the given size of the GaAs NWs, we can conclude that Si donors tend to segregate to the surface, while acceptors tend to spread within the wire. Indications of surface segregation are reported for different types of impurities in many NWs: B and P in Si unpassivated NWs (although the effect is reduced in small NWs),[24] and in (110)Ge passivated NWs,[28] Mn in (111)InP passivated NWs,[23] several different impurities in (001)Si passivated NWs.[27] Similar findings are also reported for nanocrystals.[19,41] Other impurities, such as Mn in (110)Ge passivated NWs,[25] prefer inner sites. Differences between acceptor and donor behavior have been found in the case of B and P substitutional defects in Si passivated quantum dots: B acceptor is more stable near the surface than at the center, whereas P donor prefers to stay at the interior.[20] We point out that the defect formation energy and trends can be different in passivated and nonpassivated nanostructures,[29] since passivation eliminates DBs making all the substitutional sites fourfold coordinated.

Although a systematic investigation of the energetics of dopants with respect to the NWs size is beyond our purposes, a brief comment is in order. An increase of the relative formation energy of bulklike dopants, due to quantum confinement as the size of the host decreases, has been reported for donors and acceptors in nanocrystals on the basis of SCF calculations, proposing "self-purification" mechanisms which could explain the difficulty in their doping.[17–22] Our results for donors in WZ-H(54,54) and WZ-H(96,96) indicates, however, a different trend: the relative formation energy of the Si in bulklike positions is lower in the smallest NW. This suggests that the quantum confinement effect, which would tend to increase the formation energy upon reducing the size of the wire, is not the dominant effect here. The dominant effect, instead, appears to be a surface (or surface proximity) effect (see Fig. 7). Decreasing the NW size, the donor in the inner position is at smaller distance from the surface and hence this effect acts in the direction of decreasing the relative formation energy.

B. Donor and acceptor relative stability

We address in this subsection the question of the relative stability of neutral Si donors versus acceptors in GaAs NWs, in comparison also with the bulk phase and slabs. To discuss the relative stability we consider the defects formation energy Ω_f, which for n_{Si} neutral Si atoms substituting As or Ga is[28]

$$\Omega_f = \Delta E_f - (n_{\mathrm{Si}}\mu_{\mathrm{Si}} - \Delta n_{\mathrm{Ga}}\mu_{\mathrm{Ga}} - \Delta n_{\mathrm{As}}\mu_{\mathrm{As}}), \tag{4}$$

where ΔE_f is the energy difference defined in Eq. (3), and Δn_i's are the number of Ga and As atoms substituted by Si, with $\Delta n_{\mathrm{Ga}}+\Delta n_{\mathrm{As}}=n_{\mathrm{Si}}$. In the case of an individual Si donor (d) or acceptor (a), Eq. (4) reduces to $\Omega_d=\Delta E_f-(\mu_{\mathrm{Si}}-\mu_{\mathrm{Ga}})$ or $\Omega_a=\Delta E_f-(\mu_{\mathrm{Si}}-\mu_{\mathrm{As}})$, respectively.

We first focus on the bulk case, where we have simply $E_{tot}^{undoped}=\frac{N}{2}\mu_{\mathrm{GaAs}}^{bulk}$, with N the total number of atoms in the cell. Assuming equilibrium conditions, which imply the constraint $\mu_{\mathrm{Ga}}+\mu_{\mathrm{As}}=\mu_{\mathrm{GaAs}}^{bulk}$, we can rewrite $E_{tot}^{undoped}$ as a function of the individual chemical potentials and the number of atoms n_i of type i in the doped system, since $N=n_{\mathrm{Ga}}+n_{\mathrm{As}}+n_{\mathrm{Si}}$, obtaining: $E_{tot}^{undoped}=(n_{\mathrm{Ga}}+n_{\mathrm{As}}+n_{\mathrm{Si}})(\mu_{\mathrm{Ga}}+\mu_{\mathrm{As}})/2$.

Substituting this expression in Eq. (3) and in turn in Eq. (4) we can express the defect formation energy in bulk in terms of the difference between the chemical potentials of Ga and As, $\Delta\mu=(\mu_{\mathrm{Ga}}-\mu_{\mathrm{As}})-(\mu_{\mathrm{Ga}}^{bulk}-\mu_{\mathrm{As}}^{bulk})$, and μ_{Si},[16]

$$\Omega_f(\Delta\mu,\mu_{\mathrm{Si}}) = \bar{E}_{tot}^{doped} - \frac{1}{2}(n_{\mathrm{Ga}}-n_{\mathrm{As}})\Delta\mu - n_{\mathrm{Si}}(\mu_{\mathrm{Si}}-\mu_{\mathrm{Si}}^{bulk}), \tag{5}$$

where

$$\bar{E}_{tot}^{doped} = E_{tot}^{doped} - \frac{1}{2}(n_{\mathrm{Ga}}+n_{\mathrm{As}})\mu_{\mathrm{GaAs}}^{bulk} - \frac{1}{2}(n_{\mathrm{Ga}}-n_{\mathrm{As}})(\mu_{\mathrm{Ga}}^{bulk} - \mu_{\mathrm{As}}^{bulk}) - n_{\mathrm{Si}}\mu_{\mathrm{Si}}^{bulk} \tag{6}$$

For an individual Si donor or acceptor ($n_{\mathrm{Si}}=1$), Eq. (5) reduces to

$$\Omega_{d,a}(\Delta\mu,\mu_{\mathrm{Si}}) = \bar{E}_{tot}^{doped} \pm \frac{\Delta\mu}{2} - (\mu_{\mathrm{Si}}-\mu_{\mathrm{Si}}^{bulk}), \tag{7}$$

where $+/-$ sign holds for donor/acceptor. The chemical potential difference $\Delta\mu$ varies over a range limited by the inequalities $\mu_{\mathrm{Ga}}\leq\mu_{\mathrm{Ga}}^{bulk}$ and $\mu_{\mathrm{As}}\leq\mu_{\mathrm{As}}^{bulk}$ which together with the definition of the heat of formation of GaAs, $\Delta H=\mu_{\mathrm{Ga}}^{bulk}+\mu_{\mathrm{As}}^{bulk}-\mu_{\mathrm{GaAs}}^{bulk}$, equal to about 0.8 eV from our calculations, determine the physically accessible region of $\Delta\mu$, i.e., $-\Delta H\leq\Delta\mu\leq\Delta H$.

We have calculated the formation energy of neutral Si donors and acceptors in both ZB and WZ bulk GaAs using 32-atoms supercells with one Si atom substituting one Ga or one As respectively. Our values for $\bar{E}_{tot}^{doped}$ are reported in Table II; the quantity $\Delta\Omega=\Omega_f+\mu_{\mathrm{Si}}-\mu_{\mathrm{Si}}^{bulk}$ as a function of $\Delta\mu$ is shown in Fig. 8 (first two panels from the left-hand side). Our results indicate that Si at donor and acceptor sites are basically equally favored over the accessible chemical potentials range, with donor (acceptor) site preferred in As-(Ga-) rich conditions, $\Delta\mu<0$ ($\Delta\mu>0$). For bulk ZB, our

TABLE II. Energy contribution $\bar{E}_{tot}^{doped}$ (for bulk) and $\bar{E}_{tot}^{doped} - E_s$ (for slabs and NWs, see text for the definition) to the dopant formation energy of individual Si donor and acceptor in GaAs bulk phases, slabs and NWs. Results are in eV.

System	Donor	Acceptor
Bulk ZB	1.46	1.27
Bulk WZ	1.58	1.39
$(10\bar{1}0)$ S_1 surface	1.01	1.65
$(10\bar{1}0)$ S_2 subsurface	1.08	1.22
$(11\bar{2}0)$ S_1 surface	0.92	1.69
WZ-H(54,54) NW: S_1	1.21	1.93
WZ-H(54,54) NW: S_2	1.17	1.52

results are in agreement with the findings in Ref. 16.

Similarly, we can express the formation energy in terms of $\Delta\mu$ and μ_{Si} also for slabs and NWs; however, $E_{tot}^{undoped}$ in that case is different from bulk, containing also a surface contribution $E_s: E_{tot}^{undoped}(\text{slab or NW}) = E_s + \frac{N}{2}\mu_{GaAs}^{bulk}$. Equation (7) therefore becomes

$$\Omega_{d,a}(\Delta\mu, \mu_{Si}) = \bar{E}_{tot}^{doped} - E_s \pm \frac{\Delta\mu}{2} - (\mu_{Si} - \mu_{Si}^{bulk}) \quad (8)$$

with the same definition of Eq. (6) for $\bar{E}_{tot}^{doped}$. We report $\bar{E}_{tot}^{doped} - E_s$ in Table II for donors and acceptors in surface and subsurface sites in the $(10\bar{1}0)$ WZ slab and show in Fig. 8, third panel from the right-hand side, the related quantity $\Delta\Omega$ as a function of $\Delta\mu$. We assume that the range of physically accessible region of chemical potentials for slabs and NW is the same as in bulk. We notice the large difference between S_1 and S_2 acceptor sites, S_2 being the most stable, as expected from the results reported in Fig. 7 concerning the relative stability of the different substitutional sites. For donor sites, instead, the S_1 site (trap) is slightly favored.

We complete the investigation with a NWs, focusing on the case of the WZ-H(54,54) NW. The results are reported in the last rows of Table II and in the right-hand-side panel of Fig. 8. The stability range for donor and acceptor sites is similar in bulk, slabs and NWs: there is no evidence of a dominant stability range for the occupation of acceptor sites in NWs with respect to bulk; on the contrary, in NWs the stability range for donor sites is actually increased with respect to that for acceptor sites.

Hence, we find no overall enhanced stability in NWs for As with respect to Ga substitutional sites. However, the observed *p*-type doping rather than *n*-type doping can be explained considering the preferred location within the wire of the donor and acceptor impurity. With increasing diameter, the preferential positions in the donor case become the threefold surface sites, corresponding to a deep rather than a shallow impurity that cannot be ionized at working temperature, thus suppressing the *n*-type behavior. In contrast, Si acceptors, which prefer subsurface or inner fourfold coordinated positions, can act as shallow impurities and give rise to a typical *p*-type behavior. We note that other mechanisms can have an important role in determining the *p*- or *n*-type behavior of Si-doped NWs, such as compensation mechanisms and the kinetics of Si incorporation, whose investigation however is beyond the scope of our work.

Concerning the lowering of the formation energy of Si donors when approaching the surface, it could be driven by different effects. We suggest that electronic effects could play a role, similarly to what was found for the segregation

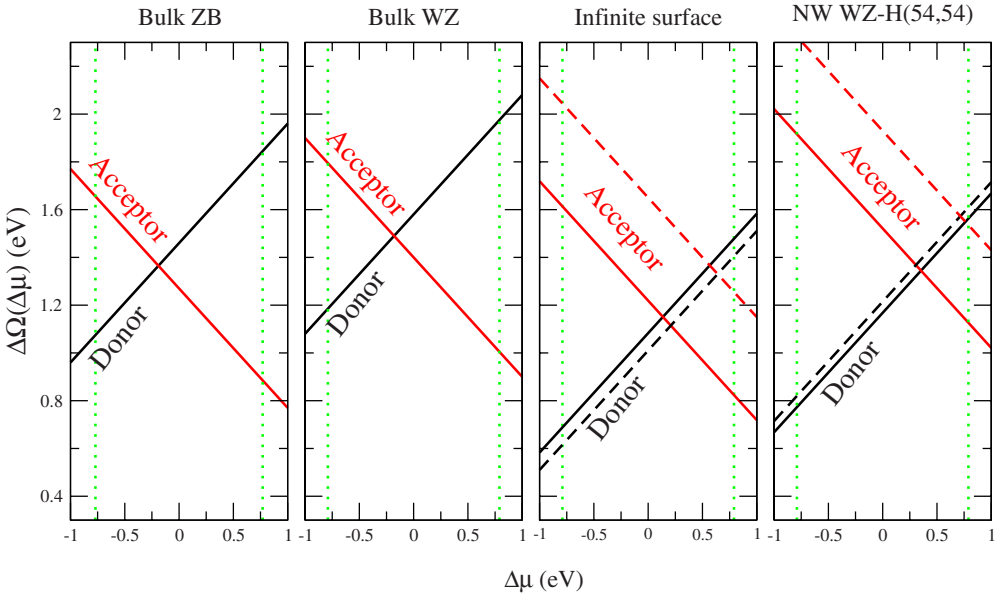

FIG. 8. (Color online) Formation energy relative to Si chemical potential, $\Delta\Omega = \Omega_f + \mu_{Si} - \mu_{Si}^{bulk}$, of Si donors/acceptors as a function of the difference $\Delta\mu$ of Ga and As chemical potentials in bulk ZB, bulk WZ, and in WZ-H(54,54) MW. The solid lines correspond to the fourfold coordinated site (S_2 site in the case of the surface and NW); the dashed lines correspond to the threefold coordinated S_1 surface site (see text) which acts as a trap for carriers. The physically accessible range of $\Delta\mu$ is indicated by the dotted lines.

of donors at semiconductor grain boundaries.[43] For the donor, mixing between low-energy conduction surface states, associated in our case with the cation surface atoms, and the hydrogenic orbital of the donor electron may cause a sizeable energy gain. For the acceptors instead, the surface As atoms are in a rather stable filled shell electronic configuration (based on the electron counting rule[44]), which is not expected to be favorable for mixing with the hydrogenic orbital of the acceptor hole. Another argument could be related to electronegativity differences. The relaxed equilibrium surface structure, with Ga inwards and As outwards, facilitate Ga dangling-bond electrons transfer to the As dangling bonds, resulting in a low-energy configuration, with empty Ga dangling bonds and fully occupied As dangling bonds. Thus, a more electropositive (electronegative) atom may be preferred at surface Ga (As) sites, but since Si electronegativity, which is in between Ga and As, is closer to Ga, this may favor surface Si impurities on Ga sites.

V. CONCLUSION

We have examined by means of first-principles calculations the stability and structural properties of intrinsic and Si-doped unpassivated GaAs NWs. For the undoped NWs, we find that NWs with diameters up to about 5 nm are more stable in the WZ form than in the ZB form. The surface density of dangling bonds plays a leading role in the stability of these NWs: for instance, ZB NWs with (112) facets, which are stoichiometric, nonpolar, but with half of the surface sites which are twofold coordinated, are the less favored among those studied. The possibility of WZ-ZB bistability for larger diameters is consistent with the experimental observations, depending on the growth mechanism.

For the Si-doped WZ NWs, we find that donors tend to segregate to the surface and acceptors to spread inside the wire. The relative stability range for donor and acceptor sites is found to be rather similar to the bulk ZB case. Actually, the stability range for donor sites in WZ NWs is slightly increased with respect to the bulk case. However, in the case of donors, and in contrast to the acceptor case, dangling-bond sites at the surface are found to be slightly favored at large diameters, thus stabilizing deep impurities rather than shallow donors. We suggest electronic effects as the possible origin of the asymmetry between donor and acceptor behavior, but the kinetics of Si incorporation may also play an important role. The prevalence of deep impurities rather than shallow donors can contribute to explain the preferential *p*-type behavior which was observed in recent experiments on Si-doped NWs grown by MBE.

Note added. Recently, after submission, two new papers concerning undoped GaAs NWs have been published.[45,46] There is good agreement between the results of these articles and ours for undoped NWs.

ACKNOWLEDGMENTS

We thank A. Franciosi, F. Jabeen, F. Martelli, and S. Rubini for fruitful discussions. We thank S. Piccinin for help with some pseudopotential tests. Computational resources have been partly obtained within the "Iniziativa Trasversale di Calcolo Parallelo" of the Italian *CNR-Istituto Nazionale per la Fisica della Materia* (CNR-INFM) and partly within the agreement between the University of Trieste and the Consorzio Interuniversitario CINECA (Italy).

[1] F. Martelli, S. Rubini, M. Piccin, G. Bais, F. Jabeen, S. De Franceschi, V. Grillo, E. Carlino, F. D'Acapito, F. Boscherini, S. Cabrini, M. Lazzarino, L. Businaro, F. Romanato, and A. Franciosi, Nano Lett. **6**, 2130 (2006).
[2] F. Martelli, M. Piccin, G. Bais, F. Jabeen, S. Ambrosini, S. Rubini, and A. Franciosi, Nanotechnology **18**, 125603 (2007).
[3] M. Piccin, G. Bais, V. Grillo, F. Jabeen, S. De Franceschi, E. Carlino, M. Lazzarino, F. Romanato, L. Businaro, S. Rubini, F. Martelli, and A. Franciosi, Physica E **37**, 134 (2007).
[4] F. Jabeen, V. Grillo, S. Rubini, and F. Martelli, Nanotechnology **19**, 275711 (2008).
[5] C. Y. Yeh, Z. W. Lu, S. Froyen, and A. Zunger, Phys. Rev. B **45**, 12130 (1992).
[6] A. Mujica, R. J. Needs, and A. Muñoz, Phys. Rev. B **52**, 8881 (1995).
[7] M. Murayama and T. Nakayama, Phys. Rev. B **49**, 4710 (1994).
[8] M. I. McMahon and R. J. Nelmes, Phys. Rev. Lett. **95**, 215505 (2005).
[9] V. G. Dubrovskii and N. V. Sibirev, Phys. Rev. B **77**, 035414 (2008).
[10] F. Glas, J. C. Harmand, and G. Patriarche, Phys. Rev. Lett. **99**, 146101 (2007).
[11] T. Akiyama, K. Sano, K. Nakamura, and T. Ito, Jpn. J. Appl. Phys. **45**, L275 (2006).
[12] T. M. Schmidt, R. H. Miwa, P. Venezuela, and A. Fazzio, Phys. Rev. B **72**, 193404 (2005).
[13] T. Akiyama, K. Nakamura, and T. Ito, Phys. Rev. B **73**, 235308 (2006).
[14] R. Leitsmann and F. Bechstedt, J. Appl. Phys. **102**, 063528 (2007).
[15] F. Jabeen, S. Rubini, and F. Martelli, Microelectron. J. **40**, 442 (2009).
[16] J. E. Northrup and S. B. Zhang, Phys. Rev. B **47**, 6791 (1993).
[17] J. Li, S.-H. Wei, and L.-W. Wang, Phys. Rev. Lett. **94**, 185501 (2005).
[18] G. Cantele, E. Degoli, E. Luppi, R. Magri, D. Ninno, G. Iadonisi, and S. Ossicini, Phys. Rev. B **72**, 113303 (2005).
[19] G. M. Dalpian and J. R. Chelikowsky, Phys. Rev. Lett. **96**, 226802 (2006); **100**, 179703 (2008).
[20] Q. Xu, J.-W. Luo, S.-S. Li, J.-B. Xia, J. Li, and S.-H. Wei, Phys. Rev. B **75**, 235304 (2007).
[21] M.-H. Du S. C. Erwin, Al. L. Efros, and D. J. Norris, Phys. Rev. Lett. **100**, 179702 (2008).
[22] J. Li, S.-H. Wei, S.-S. Li, and J.-B. Xia, Phys. Rev. B **77**, 113304 (2008).
[23] T. M. Schmidt, P. Venezuela, J. T. Arantes, and A. Fazzio, Phys.

Rev. B **73**, 235330 (2006).
[24] M. V. Fernández-Serra, Ch. Adessi, and X. Blase, Phys. Rev. Lett. **96**, 166805 (2006).
[25] J. T. Arantes, A. J. R. da Silva, and A. Fazzio, Phys. Rev. B **75**, 115113 (2007).
[26] Q. Wang, Q. Sun, and P. Jena, Phys. Rev. Lett. **95**, 167202 (2005).
[27] E. Durgun, N. Akman, C. Ataca, and S. Ciraci, Phys. Rev. B **76**, 245323 (2007).
[28] H. Peelaers, B. Partoens, and F. M. Peeters, Appl. Phys. Lett. **90**, 263103 (2007).
[29] T. M. Schmidt, Phys. Rev. B **77**, 085325 (2008).
[30] QUANTUM-ESPRESSO is a community project for high-quality quantum-simulation software, based on density-functional theory. See http://www.quantum-espresso.org and http://www.pwscf.org and P. Giannozzi, S. Baroni, N. Bonini, M. Calandra, R. Car, C. Cavazzoni, D. Ceresoli, G. L. Chiarotti, M. Cococcioni, I. Dabo, A. D. Corso, S. de Gironcoli, S. Fabris, G. Fratesi, R. Gebauer, W. Gerstmann, C. Gougoussis, A. Kokalj, M. Lazzeri, L. Martin-Samos, N. Marzari, F. Mauri, R. Mazzarello, S. Paolini, A. Pasquarello, L. Paulatto, C. Sbraccia, S. Scandolo, G. Sclauzero, A. P. Seitsonen, A. Smogunov, P. Umari, and R. M. Wentzcovitch, J. Phys.: Condens. Matter **21**, 395502 (2009).
[31] We used the pseudopotentials Ga.pz-bhs.UPF, Ga.pbe-nsp-van.UPF, As.pz-bhs.UPF, As.pbe-n-van.UPF, and Si.pz-vbc.UPF from the http://www.quantum-espresso.org distribution and a new generated one for Ga with 3*d* electrons in valence using LDA.
[32] P. B. Allen, Nano Lett. **7**, 6 (2007).
[33] WZ $(10\bar{1}0)$ surfaces can have two nonequivalent terminations, depending on whether one cuts "short" or "long" bonds (projected along $[10\bar{1}0]$) of the outermost atoms: if long bonds are cut, as in our case, only DB1 are present; if short bonds are cut, DB2 are formed. As a general rule, which is also confirmed by our calculations, a high density of DBs is unfavored, and therefore we consider only the termination corresponding to DB1s.
[34] I. Csik, S. P. Russo, and P. Mulvaney, Chem. Phys. Lett. **414**, 322 (2005).
[35] S.-P. Huang, W.-D. Cheng, D.-S. Wu, J.-M. Hu, J. Shen, Z. Xie, H. Zhang, and Y.-J. Gong, Appl. Phys. Lett. **90**, 031904 (2007).
[36] Ph. Ebert, Surf. Sci. Rep. **33**, 121 (1999).
[37] D. J. Carter, J. D. Gale, B. Delley, and C. Stampfl, Phys. Rev. B **77**, 115349 (2008).
[38] D. Vogel, P. Krüger, and J. Pollmann, Surf. Sci. **402-404**, 774 (1998).
[39] For clean InAs WZ NWs, a different energy ordering was reported in Ref. 14, namely NWs with $(10\bar{1}0)$ facets being less stable than NWs with $(11\bar{2}0)$ facets at selected diameters. This also lead to the conclusion, in Ref. 14, that for such diameters clean WZ NWs are less stable than clean ZB NWs. We believe this is because the authors of Ref. 14 included in their WZ NWs with $(10\bar{1}0)$ facets at selected diameters also facets corresponding to the "short-bond" termination of the $(10\bar{1}0)$ surface (Ref. 33), which is highly unfavorable (in particular, one can observe that opposite facets have different surface terminations in Fig. 3 of Ref. 14).
[40] Convergence tests with 14 layers give similar results.
[41] F. Iori, E. Degoli, R. Magri, I. Marri, G. Cantele, D. Ninno, F. Trani, O. Pulci, and S. Ossicini, Phys. Rev. B **76**, 085302 (2007).
[42] Different factors determine the calculated gaps reported in Table I and account for their differences. Beside the use of LDA/GGA and/or Ga 3*d* core/valence pseudopotentials for a given choice of the lattice parameter, the use of different lattice parameters by itself, whose numerical estimate can vary up to about 4% according to the approximations used, also affects remarkably the values of the gaps. In particular, our LDA estimates of the band gaps are large, at variance with usual findings, because we use the corresponding equilibrium lattice parameters which are underestimated within LDA; band gaps become smaller increasing the lattice parameter towards the experimental value. For instance, using the LDA−Ga 3*d*-core pseudopotential and the correspondent equilibrium theoretical lattice parameter we obtained an indirect energy gap for the WZ NWs studied here and a direct gap for bulk WZ. For bulk ZB we obtained an indirect gap (bottom of the conduction band close to X) of 1.38 eV and a direct gap of 1.41 eV; but using the experimental lattice parameter (5.65 a.u.), the band gap becomes direct and smaller (0.97 eV). We also checked that the overall ZB bulk band dispersion obtained with the LDA parametrization is similar to GGA, the only difference being the conduction band bottom at Γ. Further, we notice that the trend of the energy gap with the NWs size is the same whatever approximation is used. All these results make us confident about the reliability of the main findings of our work.
[43] T. A. Arias and J. D. Joannopoulos, Phys. Rev. Lett. **69**, 3330 (1992).
[44] M. D. Pashley, Phys. Rev. B **40**, 10481 (1989).
[45] M. Galicka, M. Bukala, R. Buczko, and P. Kacman, J. Phys.: Condens. Matter **20**, 454226 (2008).
[46] S. Cahangirov and S. Ciraci, Phys. Rev. B **79**, 165118 (2009).